The Journal of Chemical Physics

AIP Publishing

Surface composition of AgPd single-atom alloy catalyst in an oxidative environment

Cite as: J. Chem. Phys. **154**, 174708 (2021); https://doi.org/10.1063/5.0045999
Submitted: 31 January 2021 . Accepted: 09 April 2021 . Published Online: 05 May 2021

Caroline Hartwig, Kevin Schweinar, Rachel Nicholls, Sebastian Beeg, Robert Schlögl, and Mark Greiner

COLLECTIONS

Paper published as part of the special topic on Heterogeneous Single-Atom Catalysis

open access

View Online

Export Citation

CrossMark

ARTICLES YOU MAY BE INTERESTED IN

Isolated Pd atoms in a silver matrix: Spectroscopic and chemical properties
The Journal of Chemical Physics **154**, 184703 (2021); https://doi.org/10.1063/5.0045936

Guiding the design of oxidation-resistant Fe-based single atom alloy catalysts with insights from configurational space
The Journal of Chemical Physics **154**, 174709 (2021); https://doi.org/10.1063/5.0048698

Oxygen and vacancy defects in silicon. A quantum mechanical characterization through the IR and Raman spectra
The Journal of Chemical Physics **154**, 174707 (2021); https://doi.org/10.1063/5.0044106

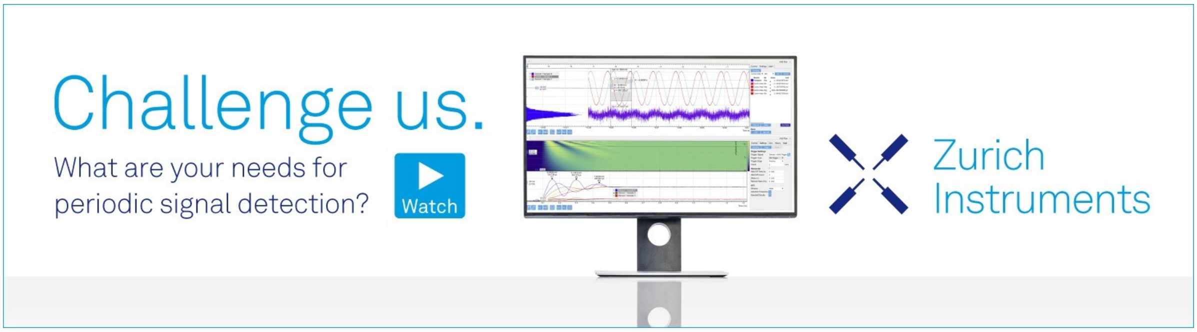

Challenge us.
What are your needs for periodic signal detection?
Watch
Zurich Instruments

© 2021 Author(s).

The Journal of Chemical Physics
ARTICLE
scitation.org/journal/jcp

Surface composition of AgPd single-atom alloy catalyst in an oxidative environment

Cite as: J. Chem. Phys. **154**, 174708 (2021); doi: 10.1063/5.0045999
Submitted: 31 January 2021 • Accepted: 9 April 2021 •
Published Online: 5 May 2021

View Online Export Citation CrossMark

Caroline Hartwig,[1] Kevin Schweinar,[2] Rachel Nicholls,[1] Sebastian Beeg,[1] Robert Schlögl,[1,3] and Mark Greiner[1,a)]

AFFILIATIONS

[1] Max Planck Institute for Chemical Energy Conversion, Mülheim an der Ruhr, Germany
[2] Max-Planck-Institut für Eisenforschung GmbH, Düsseldorf, Germany
[3] Fritz Haber Institute of the Max Planck Society, Berlin, Germany

Note: This paper is part of the JCP Special Topic on Heterogeneous Single-Atom Catalysis.
[a)] **Author to whom correspondence should be addressed:** mark.greiner@cec.mpg.de

ABSTRACT

Single-atom alloys (SAAs) have recently gained considerable attention in the field of heterogeneous catalysis research due to their potential for novel catalytic properties. While SAAs are often examined in reactions of reductive atmospheres, such as hydrogenation reactions, in the present work, we change the focus to AgPd SAAs in oxidative environments since Pd has the highest catalytic activity of all metals for oxidative reactions. Here, we examine how the chemical reactivity of AgPd SAAs differs from its constituent Pd in an oxidative atmosphere. For this purpose, electronic structure changes in an $Ag_{0.98}Pd_{0.02}$ SAA foil in 1 mbar of O_2 were studied by *in situ* x-ray photoemission spectroscopy and compared with the electronic structure of a Pd foil under the same conditions. When heated in an oxidative atmosphere, Pd in $Ag_{0.98}Pd_{0.02}$ partly oxidizes and forms a metastable PdO_x surface oxide. By using a peak area modeling procedure, we conclude that PdO_x on $Ag_{0.98}Pd_{0.02}$ is present as thin, possibly monolayer thick, PdO_x islands on the surface. In comparison to the PdO formed on the Pd foil, the PdO_x formed on AgPd is substantially less thermodynamically stable, decomposing at temperatures about 270 °C lower than the native oxide on Pd. Such behavior is an interesting property of oxides formed on dilute alloys, which could be potentially utilized in catalytic oxidative reactions such as methane oxidation.

© *2021 Author(s). All article content, except where otherwise noted, is licensed under a Creative Commons Attribution (CC BY) license (http://creativecommons.org/licenses/by/4.0/).* https://doi.org/10.1063/5.0045999

I. INTRODUCTION

During the past decade, single-atom alloys (SAAs) have gained attention in heterogeneous catalysis research due to their unique structures and potential for novel catalytic properties. A recently published review paper summarizes most of the work done so far in the field of single-atom alloy catalysis.[1] SAAs are intensively discussed in H_2 dissociation,[2–4] selective hydrogenation reactions,[5–12] and C–H activation.[13] In most reported SAA cases, the dilute, active metal is Pd or Pt substituted into a noble metal host of group 11 (Cu, Ag, and Au).[1–11] This approach has the advantage that only a small amount of the expensive active metal is used.

Several promising properties of SAAs have been reported, such as the prevention of coking,[13] the spillover of adsorbates to different active sites,[2] and improved catalytic selectivity compared to the bulk active metal. These positive effects can be explained by the fact that alloying changes the metal's properties in terms of ensemble and ligand effects. Ensemble effects refer to the change in the coordination environment of atoms on the surface, while ligand effects refer to the change in the electronic structure of metals, both of which occur upon alloying.[14]

Some ligand effects include the shifting of the metal's valence *d*-states relative to the Fermi level upon alloying, as described by the *d*-band model of Hammer and Nørskov.[15,16] These effects can be used to tune adsorbate bonding to optimize the catalytic activity.[17–20] Other ligand effects include electronic state localization, whereby weak metal–metal interaction can give rise to very localized electronic states, as reported by Greiner *et al.* in $Ag_{0.995}Cu_{0.005}$.[21] It is expected that such localized electronic states might result in catalysts that resemble homogeneous catalyst active sites.[22,23]

While these features can be engineered into an alloy via chemical synthesis, when these catalysts are put into action and exposed to reactive atmospheres, their initial structures may not be preserved. For instance, phase segregation via surface oxidation of the more oxophilic metal is known to occur when such alloys are exposed to oxidative atmospheres.[24–26] Interestingly, when oxides are formed on SAAs, the low chemical potential of the dilute solute can result in unique surface-oxide monolayers. For instance, it was reported that a metastable two-dimensional Cu oxide can form on dilute AgCu catalysts under oxidative conditions.[27] In cases where the chemical potential of the solute is high enough, bulk oxide phases form on the surface, such as Cu_2O and CuO, in the case of AgCu.[28] There is evidence that the two-dimensional Cu oxide on dilute AgCu may be responsible for the improved selectivity in ethylene epoxidation compared to pure Ag.[27,29] Thus, oxides formed on SAAs can exhibit unique properties of their own as a consequence of low solute concentration. It is important to see which ones are at play under *operando* conditions to identify structure–property relationships.

In the present work, we focus on AgPd single-atom alloys under oxidative conditions using *operando* photoemission spectroscopy. Palladium has the highest catalytic activity of all metals for oxidative reactions,[30] such as the complete oxidation of hydrocarbons in automotive exhaust catalysts and the combustion of methane in gas-powered turbines. Methane is the main component in natural gas, which can be used as fuel. Since methane has a greenhouse gas potential ∼33 times higher than that of CO_2,[31] efficient methane combustion at low temperatures is therefore crucial to avoid harmful methane emission. Usually, temperatures above 300 °C are used for Pd catalysts.[32,33]

Very important in this reaction is the oxidation state of Pd. Depending on the O_2 partial pressure and the temperature, the Pd metal can be reversibly converted to PdO, e.g., at 1 atm O_2, PdO decomposes to Pd metal at 877 °C.[34] Furthermore, it was reported that a Pd_5O_4 surface oxide forms at room temperature, which is assumed to be the precursor to PdO formation.[35–37] Many research groups observed an activity hysteresis with Pd catalysts, i.e., differing methane combustion rates when heating or cooling the catalyst.[38–40] Such observations indicate that the Pd–O system is very dynamic, which is one reason why its catalytic mechanism is still under debate, and is the focus of ongoing research. For instance, it is uncertain whether metallic Pd,[34,41] PdO,[42,43] a coexistence of both,[44–46] or a surface Pd oxide[37] is the most active phase in methane combustion.

We begin this study by examining the intrinsic oxidation behavior of Pd and AgPd by exposing them to a pure O_2 atmosphere. When AgPd is placed in an oxidizing environment, O_2-induced Pd surface segregation is expected, since Pd has a higher oxygen affinity compared to Ag. In a recent study, van Spronsen *et al.* found surface segregation of Pd in Pd/Ag(111) in 1 Torr O_2 already at 400 K.[24] Kitchin *et al.*[47] investigated the surface segregation of an $Ag_3Pd(111)$ alloy in the O_2 atmosphere using first-principles atomistic thermodynamics. Thereby, they considered the interplay between surface segregation energies, oxygen binding energies, and the gas phase chemical potential, as well as how these properties depend on the bulk alloy reservoir (Ag—or Pd rich alloy phase). Their results showed that Pd segregation is favored as the oxygen chemical potential increases, and at higher temperatures, a higher oxygen pressure is required to drive Pd surface segregation.[47,48] When Pd in the AgPd alloy is in its metallic state, Ag is preferred at the surface due to its lower surface energy and lower cohesive energy.[49–51] From those studies, it follows that the structure of an alloy surface depends on many parameters, such as the catalyst pre-treatment, the temperature, the chemical potential of the reactive atmosphere, and the composition of the alloy.

In the experiments exhibited here, $Ag_{0.98}Pd_{0.02}$ and bulk Pd are heated to temperatures ranging from 70 to 400 °C in an atmosphere of 1 mbar O_2. We found that Pd in the AgPd alloy oxidizes at substantially lower temperatures compared to pure palladium and also decomposes at lower temperatures. In-depth x-ray photoemission spectroscopy (XPS) analysis and a peak area modeling procedure suggest that a metastable PdO_x phase forms as thin, possibly monolayer thick, islands on the AgPd surface. From these observations, it is clear that the Pd-oxides formed on AgPd are considerably less stable than those formed on bulk Pd. The reason for this difference in stability is likely due to the high solubility of Pd in Ag and the lower surface energy of Ag compared to Pd. This decrease in oxide stability is expected to influence how catalytically active the alloy's surface oxygen species are and could potentially lead to, for example, methane combustion of the SAA at lower temperatures compared to pure palladium. We show that the metastable PdO_x surface oxide on AgPd is also present under methane oxidation conditions.

II. EXPERIMENTAL SECTION

A. Synthesis of the $Ag_{0.98}Pd_{0.02}$ alloy

Quantitative amounts of the Ag (slugs 3 × 3 mm^2, 99.99%) and Pd (granules < 7 mm, 99.95%) purchased from EvoChem were melted in a light oven with a four time re-melting process for homogenization. Afterward, the alloy was cold-rolled to a 1.6 mm thick foil and then annealed for 6 h at 800 °C for grain size growth. The foil was cut into smaller pieces and polished, with an incrementally finer grid, down to a 1 μm using diamond suspension. After additional Ar^+ sputtering and annealing (in O_2 and H_2 atmospheres) cycles, the grains of the polycrystalline $Ag_{0.98}Pd_{0.02}$ foil became visible under the scanning electron microscope. Through annealing in 0.5 mbar O_2 at 500 °C, impurities such as Cu, K, S, Si, and Cl came to the surface and could then be sputtered off by Ar^+ bombardment. This procedure was repeated several times to clean the sample. The last step was heating in UHV at 500 °C for recrystallization.

B. Polycrystalline Pd foil

The 0.1 mm thick Pd foil from Alfa Aesar (99.9%) was cut into a 5 × 6 mm^2 piece and subsequently cleaned by several cycles of Ar^+ sputtering and annealing [in 0.5 mbar O_2 (see above)] at 700 °C. The last step was heating in UHV at 700 °C for recrystallization.

C. *In situ* XPS study

For the *in situ* XPS measurements from which the working principle is explained elsewhere,[52] two different near ambient pressure (NAP) XPS setups were used: (i) a lab source (NAP) XPS using monochromatic Al K_α (1487 eV) radiation and a Phoibos NAP-150 hemispherical analyzer from SPECS GmbH and (ii) the (NAP) XPS setup at the UE56-2_PGM1 beamline at Bessy II, which is also equipped with a hemispherical analyzer from SPECS. In both setups,

© Author(s) 2021

the samples were heated using an IR laser from the rear, and the temperature was measured by using a K-type thermocouple fastened between the sample and a mask, which is used to fix the specimen to the sample holder.

The heating and cooling ramp of the $Ag_{0.98}Pd_{0.02}$ alloy in 1 mbar of O_2 were performed with the lab source (NAP) XPS. After Ar^+ sputter cleaning, the sample was annealed in 0.5 mbar H_2 at 450 °C for 30 min prior to oxidation in order to reach a steady state Pd surface concentration. The sample was then cooled to 70 °C, followed by taking reference spectra in vacuum. Afterward, 1 mbar O_2 was introduced and the position of the pressure regulating throttle valve was held at a fixed position. This should minimize gas expansion effects, which leads to increases in the XPS intensity at elevated temperatures, due to minimized inelastic scattering with the gas molecules.[53] As a consequence, the pressure in the XPS chamber slightly increases with the increase in temperature. The sample was heated with a very low heating speed of 0.3 °C/min from 70 to 400 °C (see Fig. 3). After the heating ramp, the sample was cooled in O_2 to 70 °C using the same ramping conditions (see Fig. 4).

To check the reproducibility of the observed behavior, this whole process was performed twice, but with a faster heating speed of 1 °C/min, and also, the pre-treatment was slightly different (0.5 mbar H_2, 400 °C, for 2 h) (see Fig. 5).

Spectra were measured during the temperature ramps using "loops," where each loop consists of a set of XPS spectra (Ag 3d, Pd 3d, O 1s, Pd $3p_{3/2}$, and S 2p). Using this procedure, one obtains a high temperature resolution. All spectra measured in the same loop are labeled using the average temperature during that loop, but since they are not recorded at the same time, the real temperature can differ by a few degree Celsius.

The drawback of this loop-procedure is that each spectrum is measured relatively quickly, and therefore, the spectra are quite noisy, but the signal-to-noise ratio can be very much improved while retaining the time resolution using principal component analysis (PCA). All XPS spectra shown in this publication are treated with the PCA noise reduction using CasaXPS 2.3.23.

To compare the oxidation behavior of AgPd with that of bulk Pd, a Pd foil was also oxidized using the laboratory source XPS. For this, the Pd foil was pre-treated in the same way as the alloy sample and afterward heated from 70 to 750 °C in 1 mbar O_2 with a temperature ramping speed of 0.4 °C/min.

TABLE I. Summary of the experiments performed for this work—the experiment IDs will be used in the main text. The results of EX4 (SM) and EX5 (SM) are shown in the supplementary material.

Experiment ID	Sample	Instrument	Oxidation conditions	Pre-treatment
EX1	Pd foil	Lab-XPS, Al K_α radiation	Heating in 1 mbar O_2, 70°C–750, 0.4 °C/min	Ar^+ sputter cleaning, reduction in 0.5 mbar H_2 at 450 °C for 2 h
EX2	$Ag_{0.98}Pd_{0.02}$	Lab-XPS, Al K_α radiation	Heating and cooling in 1 mbar O_2, 70–400 °C, 0.3 °C/min	Ar^+ sputter cleaning, reduction in 0.5 mbar H_2 at 450 °C for 2 h
EX3	$Ag_{0.98}Pd_{0.02}$	Lab-XPS, Al K_α radiation	Heating and cooling in 1 mbar O_2, 70–400 °C, 1 °C/min, several cycles	Ar^+ sputter cleaning, reduction in 0.5 mbar H_2 for 2 h
EX4 (SM)	$Ag_{0.98}Pd_{0.02}$	Synchrotron, excitation energy chosen in a way that the kinetic energy of photoelectrons is 150 eV	Heating in 1 mbar O_2, 100–326 °C, 1 °C/min	Ar^+ sputter cleaning
EX5 (SM)	$Ag_{0.98}Pd_{0.02}$	Lab-XPS, Al K_α radiation	Heating to 180 °C, various O_2 pressures (0.1 mbar, 0.3 mbar, 0.5 mbar, and 1.0 mbar), 0.7 mbar, stay at each pressure for 1 h	Ar^+ sputter cleaning
EX6	$Ag_{0.98}Pd_{0.02}$	Lab-XPS, Al K_α radiation	Heating in 1 mbar O_2:CH_4:N_2 (5:1:2), 70–500 °C, 1.0 °C/min	Ar^+ sputter cleaning
EX7	Pd foil	Lab-XPS, Al K_α radiation	Heating in 1 mbar O_2:CH_4:N_2 (5:1:2), 70–500 °C, 1.5 °C/min	Ar^+ sputter cleaning

© Author(s) 2021

Besides, the electronic structure of the Pd foil and $Ag_{0.98}Pd_{0.02}$ under methane oxidation conditions was studied. For this study, a O_2 to CH_4 ratio of 5:1 was chosen, which is the same reactant ratio that was previously reported for methane oxidation on Pd(111), studied by *in situ* XPS.[37]

Reference spectra were utilized for peak fitting. The reference spectra were measured in vacuum, and a Tougaard background was applied. Additional components that arose during the oxidation process, for which reference spectra are not available (such as suboxide species), were fit using synthetic line shapes of a Voigt form. One difficulty when analyzing these spectra is that the O 1s and Pd $3p_{3/2}$ spectra are overlapping. Additionally, O 1s spectra are, in general, difficult to fit due to the presence of different kinds of O 1s species at the same time and small binding energy differences. Therefore, one needs to add constrains on the peak position and FWHM when fitting O 1s species, but also after doing so, there is still a high uncertainty associated with the peak fit of O 1s signals.

Table I summarizes the experiments performed in this work, including the sample type, the instrument used to perform the experiment, the oxidation conditions, and the pre-treatment. In order to avoid repeating the experiment specifications in the main text, each experiment is assigned to an experiment ID, which will be used to refer to a certain experiment. The results and experimental procedure of experiments EX4 and EX5 are discussed in more detail in the supplementary material.

III. RESULTS AND DISCUSSION

A. *In situ* oxidation of pure palladium

In this work, the oxidation behavior of the AgPd single-atom alloy foil is compared with that of a polycrystalline Pd foil. Several *in situ* XPS investigations of palladium oxidation have been previously published. We summarize here the main findings from their analyses of the core-level spectra. In 2002, Lundgren *et al.* found, by a combination of STM, surface XRD, high resolution XPS, and density functional theory (DFT) calculations, a metastable two-dimensional Pd_5O_4 surface oxide species, where the corresponding Pd $3d_{5/2}$ emission line consists of two peaks at 335.5 eV and 336.2 eV with a ratio of 4:1 on a Pd(111) single crystal.[35] The corresponding two O 1s lines have a ratio of 1:1 and are threefold and fourfold coordinated to Pd. *In situ* XPS oxidation studies of Pd(111) reveal that this Pd_5O_4 surface oxide is the precursor species for the bulk PdO phase.[36,54] The XPS signals related to the Pd_5O_4 species were labeled Pd-ox(I) and Pd-ox(II) (in the Pd $3d_{5/2}$ spectral region), as well as O(I) and O(II) (in the O 1s spectral region). The same peak labels are used in this work. In that study, the Pd-ox(II) signal was allowed to shift to become the bulk PdO species.[54] Ketteler *et al.* tried to experimentally determine, by *in situ* XPS, the phase diagram of Pd(111) as a function of the pressure and temperature. Thereby, the high dynamic of the Pd/O system became evident, since they found chemisorbed oxide phases, surface oxides, possible sub-surface oxides, and bulk PdO.[55]

Figure 1 shows the *in situ* XPS spectra of Pd oxidation from the present study. The plots show the Pd 3d, Pd $3p_{3/2}$, and O 1s spectra of the polycrystalline Pd foil during a heating ramp in 1 mbar of O_2 (EX1). The temperature starts at 160 °C in this analysis because below that temperature, carbon contaminations, originating from hydrocarbons sticking to the side walls of the XPS chamber and which lead to additional signals[56–58] that are not relevant for this analysis, were present.

In the Pd 3d spectrum, three species could be differentiated: Pd metal, Pd-ox(I), and Pd-ox(II). Pd-ox(I) and Pd-ox(II) are assigned to a surface oxide precursor species, whereby, in the fitting procedure, the Pd-ox(II) peak is allowed to shift a bit as it transitions into

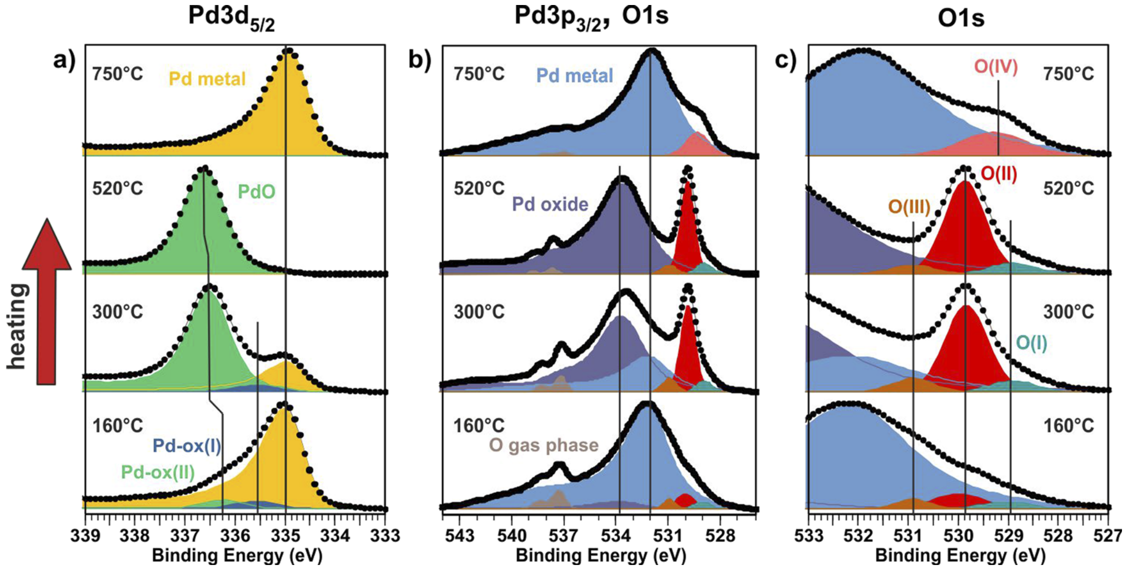

FIG. 1. Pd $3d_{5/2}$ (a) and Pd $3p_{3/2}$, O 1s (b) and (zoomed) O 1s XPS spectra (c) of the Pd foil during heating in 1 mbar O_2. The black circles represent the measured points after PCA noise reduction and background subtraction. Note that the ordinate axis in the spectra is normalized to maximum intensity.

© Author(s) 2021

the bulk PdO species. The binding energy for those core-level species is consistent with previous reports of Pd oxidation.[35,54,55]

The O 1s signals overlap with the Pd $3p_{3/2}$ signal and the O 1s gas phase signal [Fig. 1(b)], which makes precise analysis of the oxygen species challenging. Using the Pd $3p_{3/2}$ signal from the reduced state of Pd measured in vacuum as a reference spectrum, we can differentiate between the peaks of the metal and the oxide. With the help of previous O 1s peak models from the published literature, we distinguish four O 1s species: O(I), O(II), O(III), and O(IV).[54,59,60]

Before going into the details of the chemical characteristics of each species, we will have a closer look on how the peak areas change with temperature. Figure 2 shows line profiles, representing the XPS peak areas of each species documented here, as a function of time. We define the "onset oxidation temperature" (OOT) here as the intercept between the baseline and the line of the steepest slope of the line profile. In the same manner, the "onset oxide decomposition temperature" (OODT) is defined. During heating, the OOT is at around 240 °C. This is the point where PdO begins to grow on the surface. The PdO layer becomes at least 4.5 nm (3λ) thick, as inferred from the fact that no more Pd metal signal could be detected at 440 °C. At 590 °C (OODT), PdO decomposes very rapidly to Pd metal.

Concurrent with the formation and decomposition of PdO, the O(II) signal increases and decreases, respectively [Fig. 2(b)]. This correlation between peak intensities is used to infer that the O(II) component represents the oxygen species of the PdO phase (i.e., lattice oxygen).

In the Pd-ox(II) and O(II) line profile of Fig. 2(b), one can observe a plateau below 240 °C. This plateau in intensities of these features indicates that the O(I), O(III), and Pd-ox(I) species have already formed [Fig. 2(c)]. In agreement with previous literature studies, this observation would suggest that, under these conditions, the oxide precursor species has already formed on the surface. The corresponding peak positions of Pd-ox(I) (335.55 eV), Pd-ox(II) (336.2 eV), O(I) (528.9 eV), and O(II) (529.8 eV) match well with the 2D Pd_5O_4 precursor species.[35,54] However, in the line profile [Fig. 2(c)], one can see that the area ratio of Pd-ox(I) to Pd-ox(II) (below 240 °C) is substantially different from the previously reported 4:1 ratio.[35] In the present dataset, Pd-ox(II) has even a higher concentration than Pd-ox(I). We attribute this discrepancy to the fact that the sample investigated here is poly-crystalline, while the Pd_5O_4 surface oxide reported previously was from Pd(111).[35] It is expected that different metal surface orientations can form monolayer-oxides of differing stoichiometries, differing symmetries, and, consequently, differing XPS peak ratios. Additionally, oxygen can also adsorb disorderly (e.g., on step edges), which influences the Pd $3d_{5/2}$ peak ratio.[54,55] Furthermore, a kinetic XPS study of Pd oxidation found that the PdO nucleation on Pd(110) proceeded at ~100 °C lower temperatures than on Pd(111).[59] XPS just provides an average electronic structure, and therefore, it might be possible that the Pd oxidation toward PdO may be more progressed on some grains than on others, which also affects the Pd-ox(I) to Pd-ox(II) ratio.

As the temperature increases further, the Pd-ox(II) signal shifts from 336.2 eV to 336.6 eV, and the intensities of the Pd-ox(I) and Pd metal species decrease. At 410 °C, only the Pd-ox(II) signal is present, indicating that a thick film of bulk PdO has formed on the surface. The O 1s spectrum of the PdO species exhibits two peaks:

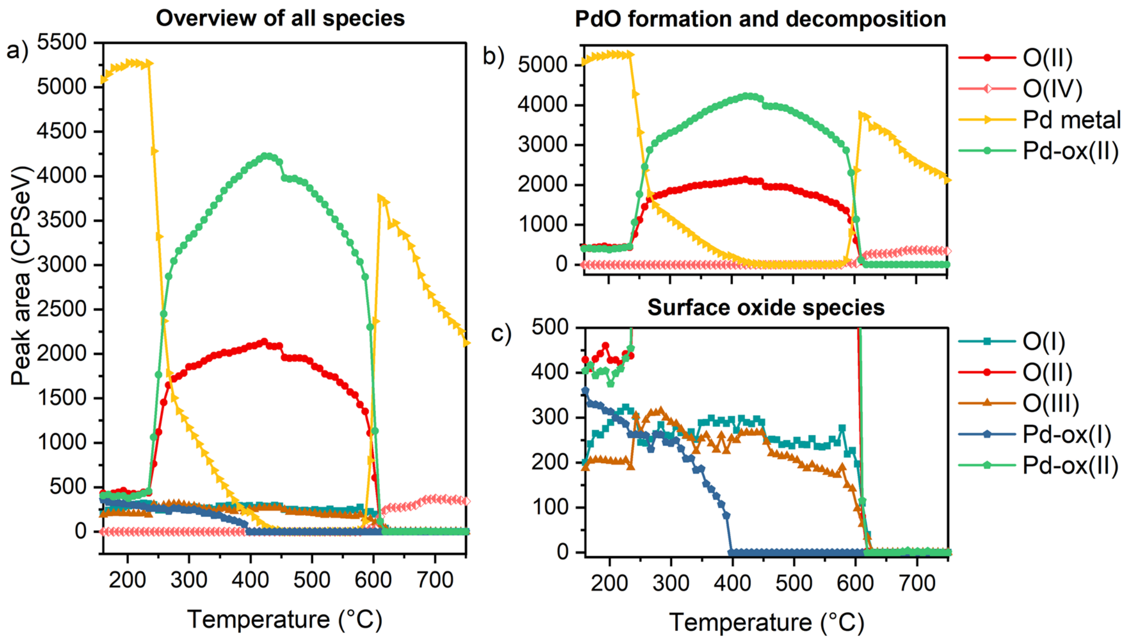

FIG. 2. (a) Peak area line profile of all relevant synthetic components as a function of temperature during heating of a polycrystalline Pd foil in 1 mbar O_2. (b) Peak area line profile of the Pd metal, Pd-ox(II), O(II), and O(IV), which shows the main trend of PdO formation and decomposition. (c) Line profile of the less intensive synthetic components O(I), O(II), O(III), Pd-ox(I), and Pd-ox(II), which represent surface oxide species.

© Author(s) 2021

O(I) at 528.9 eV and the more intense O(II) at 529.8 eV. Depth profiling indicates that O(I) originates from an oxygen-terminated PdO surface.[55] The line profile in Fig. 2 shows that, from the beginning of the temperature ramp until the point where PdO decomposes, this O(I) species is present and has a constant peak area. After PdO has completely decomposed, the O(I) species is no longer present. These observations are consistent with the interpretation that the O(I) species is due to an oxygen-terminated surface. The O(II) species, on the other hand, has the same binding energy as one of the precursor species; however, it strongly increases when PdO begins to form, which is consistent with the interpretation that O(II) is from lattice oxygen in PdO.

In addition to these two oxide-related species, we observe an O 1s species at 530.9 eV [O(III)]. An oxygen species of this binding energy on Pd has also been previously reported[59,60] and was attributed to hydroxyl groups.[60] Hydroxyl formation is also very likely in our case, since the sample was pretreated in H_2, which can lead to some PdH formation. The hydrides of PdH may then later bind to oxygen. The O(III) species also disappears as PdO decomposes, around 600 °C, and during this process, another O 1s species arises at 529.3 eV [O(IV)]. A species of this binding energy has previously been suggested to be dissolved oxygen;[54] however, impurities bound to oxygen could also be a candidate for this species.

It should be noted that in the present work, we measured Pd oxidation with an Al K_α source (1487 eV), which is less surface sensitive than the photon energies used in the cited Pd oxidation studies, measured with synchrotron radiation. Therefore, we are less sensitive for surface oxide species, leading to very low signal intensities and consequently to uncertainties and fluctuations in the peak fit.

B. *In situ* XPS oxidation of AgPd at 1 mbar

For comparison with the oxidation of bulk Pd, we performed an identical heating ramp, in O_2, on an AgPd single-atom alloy. The behavior of the chemical species on the surface is quite complex, as multiple chemical species are present simultaneously, and their relative concentrations change dynamically during the temperature ramp. We provide a detailed discussion on identifying the many peaks observed in the XPS spectra; however, the most clear and obvious take-away from this investigation is as follows: When the AgPd SAA is heated in O_2, the Pd becomes preferentially oxidized and forms an oxide over-layer, similar to the case of bulk Pd oxidation; however, the oxide formed on the AgPd SAA does not form a thick layer, and it thermally decomposes at a much lower temperature (~270 °C lower) than does the oxide formed on Pd.

Before going into detail about the oxidative properties of $Ag_{0.98}Pd_{0.02}$, it is important to mention that we validated the homogeneous distribution of Pd in the Ag host by spectroscopic methods to ensure that the alloy is indeed a SAA (see Fig. S1).[61] Figure 3 shows the Pd 3d, O 1s/Pd $3p_{3/2}$, and Ag 3d spectra measured during the heating ramp in 1 mbar O_2 (EX2). Figure 4 represents the same spectral regions during the cooling ramp. Noise reduction using PCA was performed on these spectra in order to achieve both time resolution and signal quality. After applying PCA noise reduction on the cooling data, some sulfur impurities could be detected that were not present during heating, and because of the low signal-to-noise ratio of the S 2p signal, there is a high uncertainty associated with its intensity and line shape. Note that silicon, which is a very common impurity in Ag, could not be detected during heating and cooling in O_2.

As the temperature increases beyond 100 °C, an oxidized form of Pd becomes apparent in the Pd 3d spectrum, with the appearance of a peak at 336.35 eV (i.e., shifted 1.3 eV to higher binding energy compared to the metallic Pd peak at 335.05 eV). As the temperature goes beyond 320 °C, the Pd oxide thermally decomposes, leaving behind metallic Pd, as shown in Fig. 3(a). Note that this temperature

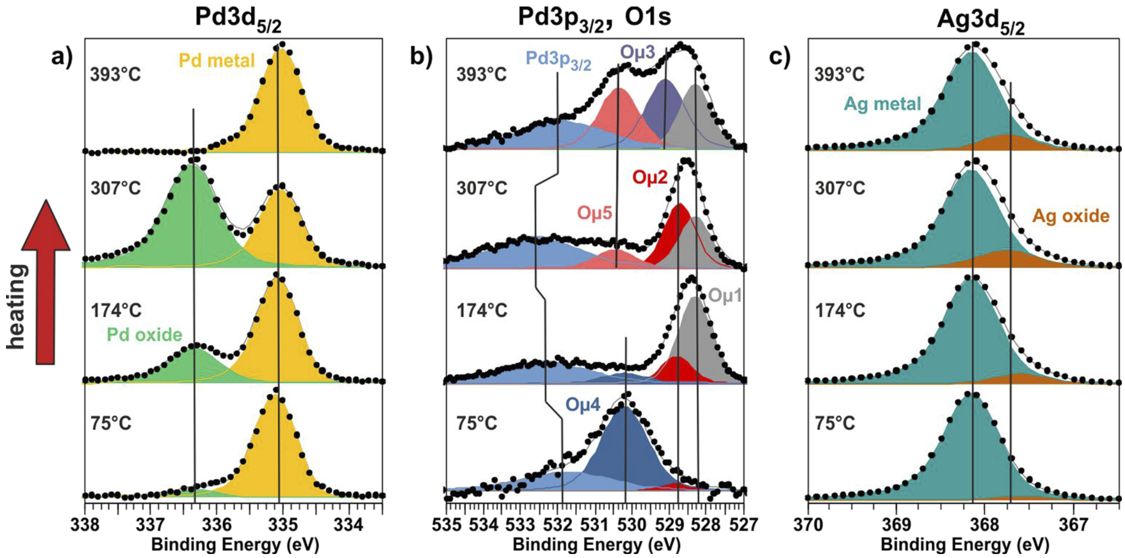

FIG. 3. Comparison of XPS spectra of (a) Pd $3d_{5/2}$, (b) Pd $3p_{3/2}$/O 1s, and (c) Ag $3d_{5/2}$ during heating in 1 mbar O_2 from 70 to 400 °C. The black circles represent the measured points after PCA noise reduction and background subtraction; the gray envelope is the sum of the synthetic compounds. The ordinate axis in the spectra is normalized.

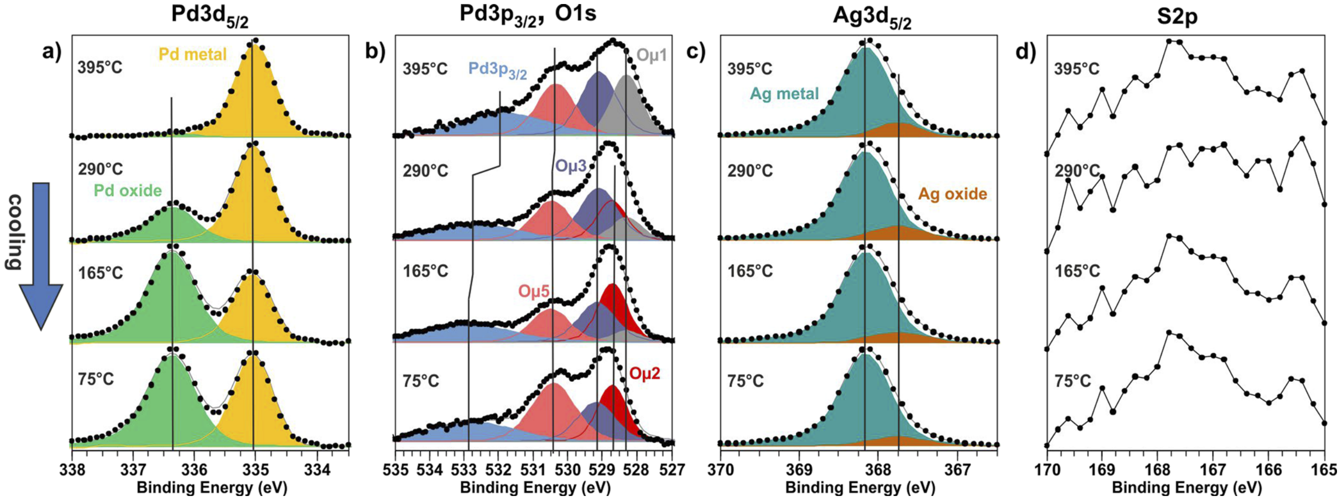

FIG. 4. Comparison of spectra during cooling in 1 mbar O_2. (a) Pd $3d_{5/2}$, (b) O 1s and Pd $3p_{3/2}$ spectra, (c) Ag $3d_{5/2}$ spectra, and (d) S 2p spectra. The black circles represent the measured points after PCA noise reduction and background subtraction; the gray envelope is the sum of the synthetic compounds. The ordinate values of the spectra are min-to-max normalized.

is ~270 °C lower than the temperature at which PdO decomposed on bulk Pd.

After decomposition of the oxidized Pd species, the sample was cooled to room temperature at a constant rate. During cooling, the Pd oxide re-forms, with a hysteresis in formation temperature, whereby the oxide begins to form at a lower temperature than the temperature at which it decomposed during the heating ramp. Additionally, the oxide persists after cooling to room temperature in oxygen [Fig. 4(a)] and remains stable in vacuum.

The hysteresis in oxide stability temperature, during heating and cooling, can be clearly seen in line profiles in Fig. 5 (EX3), where the peak area of the Pd metal and Pd oxide is plotted as a function of temperature. As shown here, Pd begins to oxidize at 70 °C, reaches its maximum intensity at 295 °C, and becomes fully decomposed by 375 °C. During cooling, the oxide begins to re-form at an OOT of 335 °C, reaching its maximum intensity at 220 °C, after which its intensity remains constant. The Pd oxide signal intensity during cooling is observed to be higher than that during heating. When heating the sample for a second time, the Pd oxide OODT is at 285 °C, that is, 15 °C lower than that during the first heating ramp. The complete decomposition, however, is reached at the same temperature in both cases [Fig. 5(a)].

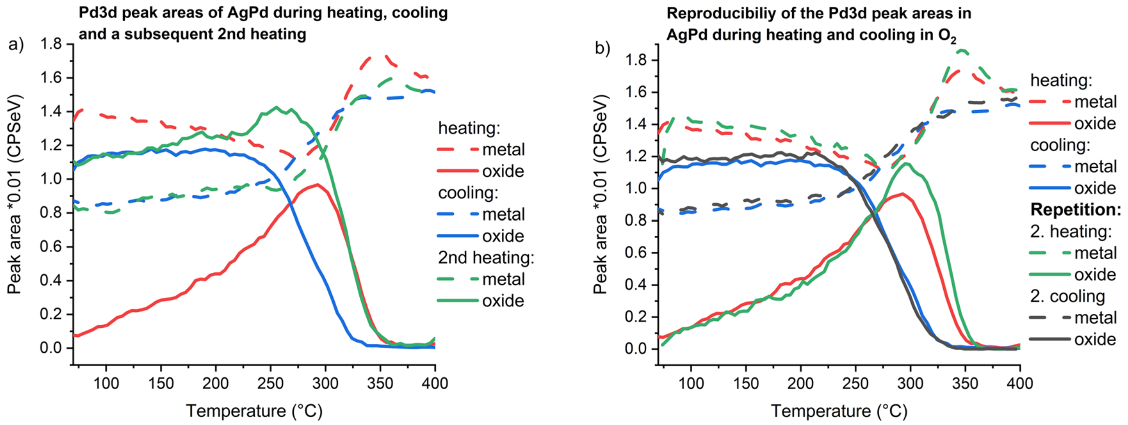

FIG. 5. The graphs represent the intensity of the Pd oxide and the Pd metal Pd 3d peak as a function of the temperature during heating and cooling of $Ag_{0.98}Pd_{0.02}$ in 1 mbar O_2. In panel (a), a second heating was performed directly after the cooling, whereas in panel (b), the reproducibility was tested by performing the same heating and cooling experiment twice and the sample had the same sputter and reduction pre-treatment in each run.

© Author(s) 2021

In Fig. 5(b), the same pre-treatment and heating and cooling ramp were repeated. During cooling, the results are very reproducible, as shown by the overlap between the black and blue profiles in Fig. 5(b). During the second heating, a slightly higher Pd oxide intensity is measured (green solid line). The main outcome of the line profiles in Fig. 5 is that the heating and cooling experiment in oxygen can be well reproduced.

After having discussed how the Pd 3d species change with temperature, we will now have a closer look onto the O 1s species to see how they correlate with Pd oxide formation. The investigation of the O 1s species is the most complex of the analyses because of the many oxygen species present on the surface. In Fig. 3(b), one can see that we fitted the Pd $3p_{3/2}$/O 1s spectrum using six different species, which have only slight binding energy differences. The use of so many peaks is problematic because it means that there is a high degree of uncertainty in the fitting model. Unfortunately, this is a fact one must live with in this case because prior knowledge of Ag and Pd in oxygen tells us that at least five species of oxygen could form, e.g., oxygen from Ag_2O, PdO, and Pd_5O_4 and from several O-adsorbate configurations on Ag and on Pd (as well as oxygen bound to impurities). Additionally, all the O 1s peaks are overlaid on top of the Pd $3p_{3/2}$ peak, which complicates the analysis even further.

Depending on the degree of Pd oxide on the surface, the Pd $3p_{3/2}$ peak shifts between 531.8 eV (metallic) and 532.9 eV (mixture of Pd metal and oxide). A differentiation between Pd $3p_{3/2}$ metal and the Pd $3p_{3/2}$ oxide component was not possible due to the high FWHM of the peak and small chemical shift between the two states.

Based on a peak model that remains consistent for all data in the dataset, we arrive at five different O 1s species (Oμ1, Oμ2, Oμ3, Oμ4, and Oμ5). It is worth mentioning that in the literature about Ag–O species, one often distinguishes between "electrophilic" (O_{elec}) and "nucleophilic" (O_{nuc}) oxygen species.[62,63] The binding energies of the Oμ1, Oμ2, and Oμ3 species lay in the region of the nucleophilic O 1s species, and Oμ3 and Oμ4 have binding energies similar to the electrophilic oxygen species. It is important to note that there are even more possible oxygen species related to Pd,[54] Ag,[64] or impurities,[64,65] which we possibly could not detect with certainty due to very little differences in the chemical shift, and a lower surface sensitivity compared to measurements using synchrotron radiation.

Figure 6 shows the trends in peak area, for all species measured, as a function of time during the temperature ramp. The line profile in Fig. 6(b) shows that the Oμ2 (528.7 eV) increases when the Pd oxide forms and disappears after the Pd oxide decomposes. This correlation suggests that the Oμ2 species is from the Pd oxide. At a lower binding energy, there is the Oμ1 signal (528.3 eV), which is still present after the Pd oxide has decomposed. Additionally, a Oμ3 signal at 529.1 eV arises as the Pd oxide decomposes. Furthermore, there is a relatively intense Oμ4 (530.2 eV) below 120 °C during heating.

This Oμ4 (530.2 eV) species at low temperatures can be assigned to disordered atomically adsorbed oxygen on Ag, as previously reported.[66] The peak area at 530.2 eV is low at temperatures between 130 and 280 °C and then increases again at temperatures greater than 300 °C. We assume that the peak that forms at temperatures greater than 300 °C is actually a chemically distinct species

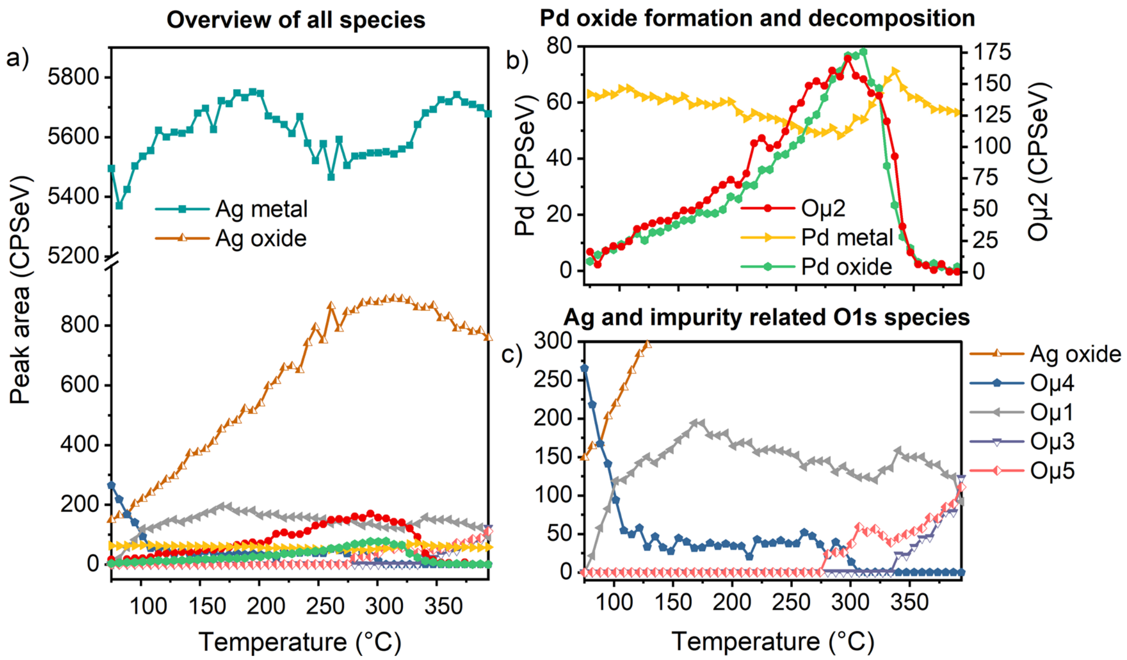

FIG. 6. (a) Peak area–line profile of all relevant synthetic components of $Ag_{0.98}Pd_{0.02}$ as a function of temperature during heating in 1 mbar O_2. (b) Temperature–line profile showing the formation and decomposition of the surface Pd oxide. Oμ2 is plotted with its own y-scale to better see the correlation with Pd oxide. (c) Profile of the O 1s species, which are related to Ag or impurities.

© Author(s) 2021

from Oμ4. Thus, we introduce a species labeled Oμ5, which has a very similar binding energy to Oμ4 but represents a different chemical entity. This interpretation is reasonable, since atomically adsorbed oxygen on Ag is unstable at temperatures above 300 °C; however, the actual transition temperature from Oμ4 to Oμ5 is uncertain, since these peaks are highly overlapped [Fig. 6(c)].

From the broadening of the Ag 3d$_{5/2}$ signals [Fig. 3(c)], it is apparent that Ag oxide species are present on the surface.[64] To fit this line shape, a reference spectrum of Ag 3d in the reduced state was chosen, and an oxide component was added to the low binding energy side, which was allowed to shift between 367.6 eV and 367.75 eV. The intensity of the Ag oxide increases until 300 °C and, afterward, decreases slightly.

The position of Oμ1 of 528.3 eV is consistent with the reported binding energy of the common Ag–O reconstruction, called p(4 × 4)-O reconstruction on a Ag(111) surface (528.1 eV,[66] 528.3 eV,[64] and 528.2–528.5 eV[65]). Consistent with this interpretation, we see that both Oμ1 and Ag oxide signals are correlated and increase together at temperatures below 170 °C [Fig. 6(c)]. At higher temperatures, the Oμ5 and Oμ3 species form. These species might also correlate with the Ag oxide intensity. Additionally, the number of Pd neighbors influences the broadening of the Ag.[24,60] The coordination number might change as Pd segregates to the surface to become oxidized. Consequently, a high uncertainty is associated with the intensity and chemical shift of the Ag oxide component. The Oμ3 species has a binding energy of 529.1 eV and this is in agreement with an oxide species on a Ag surface called Oα_2.[64] The origin of this species is still unknown. It is known that the signal increases with higher temperatures and is unstable in an inert atmosphere or vacuum.

At this point of analysis, no clear correlations between the Ag and Pd oxide and the Oμ5 species at 530.3 eV could be drawn, which leads to the assumption that it could be an impurity related oxide. Impurities and foreign atoms such as Pd segregate to the surface of Ag in an oxidative atmosphere, and thereby, they form nanostructures or even build layered structures when they wet the oxidized Ag surface. In this study, it seems that the Pd oxide wets the Ag surface oxide. Besides Pd 3d and O 1s, a very weak S 2p signal was measured during cooling [see Fig. 4(d) and the temperature-line profile in Fig. S2]. On a Ag(111) surface, adsorbed SO$_4$ is supposed to have a binding energy of 530.2 eV and a SO$_4$ induced reconstruction, called [(7 × $\sqrt{3}$)rect] a binding energy of 530.7 eV.[65] Hence, we assume that the Oμ5 species is correlated with the S 2p signal. Since the lab XPS spectrometer with Al K$_\alpha$ radiation has a very low sulfur sensitivity, the S 2p signal intensity highly fluctuates, and no clear temperature trend could be observed.

In order to verify the correlation between the Oμ5 species and SO$_4$ formation on the surface, similar measurements were performed using synchrotron radiation (EX4), which enables a much higher surface sensitivity compared to Al K$_\alpha$ radiation, since the photon energy can be tuned.

The main outcome of the oxidation of Ag$_{0.98}$Pd$_{0.02}$ using synchrotron radiation is that a pronounced S 2p peak could be detected with the increase in temperature, which is linearly correlated with the formation of the Oμ5 species. Additionally, the valence band was investigated showing corresponding S 3p and O 2p species. The binding energies of the S 2p and Oμ5 species verify that indeed, a SO$_4$ induced reconstruction has formed (see Figs. S3 and S4).

C. Comparison of the Ag$_{0.98}$Pd$_{0.02}$ oxidation with pure palladium

The oxidation behavior of Pd in AgPd and bulk Pd is similar in the sense that, in both cases, Pd begins in a metallic state and then forms a Pd-oxide on the surface, followed by thermal decomposition at higher temperatures. The most striking difference between the two cases is that the thermal decomposition temperature differs by ∼270 °C. That is, the Pd-oxide formed on AgPd decomposes at a temperature of 270 °C lower than the oxide formed on Pd. This difference will be emphasized here with a comparison of the Pd 3d oxide and metal signals from the two samples (polycrystalline Pd foil and the AgPd SAA foil), as shown in Fig. 7. It was found that the Pd oxide on the AgPd alloy decomposes already around 320 °C, whereas the PdO oxide formed on bulk Pd decomposes at 590 °C.

In addition, the onset of Pd oxidation exhibits differences between AgPd and Pd. On AgPd, the Pd oxide signal begins to form at a low temperature and slowly but continuously increases with temperature because this is a kinetic diffusion limited process. The diffusion is enhanced at higher temperature, and as a consequence, a fast slope of Pd oxide formation is expected when the oxidation is performed at a higher starting temperature (e.g., 300 °C). In contrast, on the Pd metal, the precursor species [Pd-ox(I) and Pd-ox(II)] formed at low temperature, remain stable, and roughly constant in intensity, and until at ∼240 °C, there is an abrupt phase transition from the PdO precursor species to PdO. It seems that at 240 °C, the reaction barrier for PdO seed formation is overcome, and afterward, PdO grows gradually in thickness. The PdO decomposes rapidly around 590 °C to Pd metal without re-forming the intermediate oxide phase.[55] The Pd oxide decomposition on AgPd occurs over a longer temperature range compared to PdO on Pd. The diffusion of Pd into the Ag bulk when the Pd oxide decomposes is still diffusion limited but is enhanced compared to the oxide formation due to the higher temperature. Note that both samples are

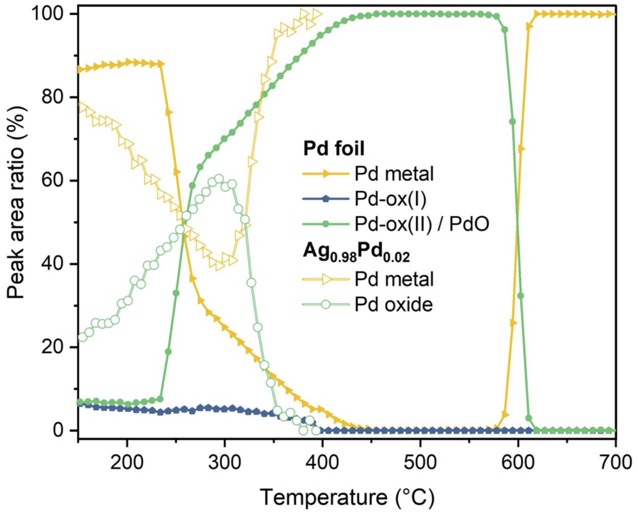

FIG. 7. Comparison of the area ratio profile of the Pd 3d metal and oxide peak of the Ag$_{0.98}$Pd$_{0.02}$ alloy with the polycrystalline Pd foil depending on the temperature during heating in 1 mbar O$_2$.

© Author(s) 2021

polycrystalline, and therefore, it might be possible that the oxide formation and decomposition occur on grains with different crystal orientations at different temperatures[59] which lead to less sharp phase transitions than that on single crystals. Additionally, the exact transition temperatures and their temperature range depend on the heating rate.

These observations reveal that the AgPd SAA exhibits substantially different behavior in terms of both formation and thermodynamic stability than that by PdO formed on bulk Pd. One might therefore expect that it could also have different catalytic properties.

While the trends in oxide formation and decomposition temperature on PdO formed on the Pd metal vs the oxidized Pd formed on AgPd show clear differences in behavior, we more closely examined their respective XPS binding energies for further evidence of differences in the electronic structure. Table II compares the measured binding energies of the different $Ag_{0.98}Pd_{0.02}$ XPS species with the characteristics of the polycrystalline Pd foil. Note that the chemical species in the table are all intermediates, which are present in the O_2 atmosphere and might not be thermodynamic stable phases.

From the peak positions listed in Table II, we can see that the Pd $3d_{5/2}$ peak position from the metallic state of Pd in AgPd is very similar to that of the metallic state of bulk Pd. The oxidized form of Pd on AgPd also has a very similar binding energy to that of PdO formed on bulk Pd (336.35 eV vs 336.2–336.6 eV, respectively). The O 1s binding energy of the O-species in the oxide formed on AgPd, however, is very similar to the surface-terminated species from PdO (528.7 eV vs 528.9 eV, respectively).

Thus, at first glance, the XPS data do not indicate any strong differences in electronic structure between the oxide on AgPd and PdO. However, when one considers core-hole screening effects, the interpretation changes. Consider that the oxide on AgPd is a very thin film. This means that when an electron hole is generated during photoemission, the hole is screened by the electron density of the surrounding material. In this case, the surrounding material is a metal, and screening is very efficient. When a hole is generated in a bulk oxide, the environment around the hole is an oxide. Oxides typically have lower free-electron density than metals. Thus, one would expect weaker core-hole screening in the bulk oxide.

Core-hole screening influences the XPS binding energy. A photoemission event that gives rise to a well-screened hole results in a peak with a lower binding energy than a photoemission event (from the same initial state) where the core-hole is poorly screened. Thus, even though Pd $3d_{5/2}$ binding energies from oxidized AgPd and PdO are very similar, it could be that the Pd centers have substantially different initial states (i.e., different ground state electronic structures).

If we assume that core-hole screening is more effective in the case of oxidized AgPd and less effective in the case of PdO, then the observation of identical binding energies would imply that the Pd in oxidized AgPd possesses lower electron density that the Pd sites in PdO. Unfortunately, without *a priori* knowledge of the precise atomic structure of the oxidized AgPd surface, we cannot simulate the charge density on the atoms to confirm this assumption.

The screening effects from the underlying metal would give rise to the same effects in the O 1s signals. When we compare O 1s binding energies of oxidized AgPd (the Oμ2 species) with the corresponding species for PdO on Pd [the O(II) species], we note that the O 1s binding energy on AgPd is 0.9 eV lower in (528.7 eV vs 529.6 eV, respectively). If we again assume that the stronger core-hole screening in the case of oxide on AgPd shifts the O 1s peak to lower binding energy, then one could infer that the initial states of the oxygen species are similar in both cases of oxidized AgPd and PdO.

TABLE II. XPS binding energies of Ag $3d_{5/2}$, Pd $3d_{5/2}$, and O 1s of $Ag_{0.98}Pd_{0.02}$ and a Pd foil during oxidation—the peaks are assigned to their chemical origin by considering different references.

Sample	Conditions	Emission line	BE (eV)	Label	Interpretation	References
$Ag_{0.98}Pd_{0.02}$	Heating and cooling in 1 mbar O_2, 0.3 °C/min, Lab-XPS (EX2)	Ag $3d_{5/2}$	368.18	Ag metal	Metal	60 and 64–66
			367.6–367.8	Ag oxide	Oxide	60 and 64–66
		Pd $3d_{5/2}$	335.05	Pd metal	Metal	30
			336.35	Pd oxide	Oxide	
		O 1s	528.3	Oμ1	Ag–O reconst.	60 and 64–66
			528.7	Oμ2	Surface Pd oxide	
			529.1	Oμ3	Unknown Ag oxide related species	64
			530.2	Oμ4	Atomically adsorbed O	60 and 64
			530.3	Oμ5	Adsorbed SO_4, SO_4 induced reconst.	65
Pd foil	Heating and cooling in 1 mbar O_2, 0.4 °C/min, Lab-XPS (EX1)	Pd $3d_{5/2}$	335.0	Pd metal	Metal	35, 36, 54, and 55
			335.55	Pd-ox(I)	PdO precursor	35, 36, 54, and 55
			336.2–336.6	Pd-ox(II)	PdO precursor and PdO	35, 36, 54, and 55
		O 1s	528.9	O(I)	Precursor, surface oxides in PdO	36 and 55
			529.8	O(II)	Precursor, PdO	36, 54, and 55
			530.9	O(III)	Hydroxyls	59 and 60
			529.3	O(IV)	Unknown	54

© Author(s) 2021

In Sec. III D, we investigate in more detail the energetic effect leading to Pd oxide formation on the AgPd SAA and why the Pd surface oxide decomposes at lower temperatures compared to PdO on a Pd foil.

D. Surface segregation of Pd in the AgPd SAA alloy

Based on the XPS peak intensities, we have, until now, assumed that the Pd oxide formed on AgPd is a very thin film, possibly monolayer thick, and similar to oxide monolayers reported for previous dilute alloy systems.[27] To substantiate this belief, we present here a more detailed analysis of the XPS peak intensities. Through this analysis, we arrive at a model for the surface morphology, which suggests that the Pd oxide that formed on AgPd consists of two-dimensional PdO_x islands on top of the Ag oxide, resulting in the depletion of Pd from the sub-surface regions. Hence, the AgPd SAA is an excellent precursor for a metastable state, which may not be possible to produce with other starting compositions, since the oxidation of conventional alloys would lead to immediate phase segregation and the formation of Pd nanoparticles.

Figure 8 shows how the total relative intensity of Pd changes through the oxidation and decomposition process (EX3). When oxidation starts, the metal peak decreases, and the oxide peak increases. Considering the total Pd signal, one can see that the Pd intensity raises as Pd becomes oxidized. This finding suggests that Pd surface segregation may be taking place. As the oxide decomposes again at higher temperatures, the total Pd intensity returns to approximately the same value as that before oxidation. This observation proposes that the reduced Pd diffuses back into the Ag interior upon reduction. During cooling in oxygen, again Pd oxidation and surface segregation take place.

The presumed surface segregation of Pd, as inferred from the increase in intensity, can be explained by the higher oxygen affinity of Pd compared to Ag, leading to adsorbate-induced surface segregation,[67] whereas the migration of Pd into the Ag bulk after the Pd oxide decomposes can be well explained by the more noble nature of Ag and, therefore, a lower surface energy.[49–51]

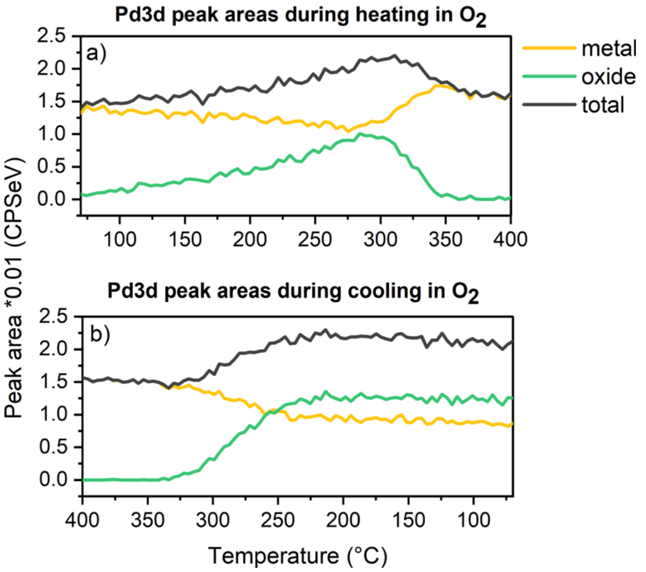

FIG. 8. Pd 3d peak areas of AgPd SAA [Pd 3d metal, Pd 3d oxide, and the sum of both (total)] as a function of time: (a) during heating and (b) during cooling in 1 mbar O_2.

Kitchin *et al.*[47] found by their theoretical investigations of the $Ag_3Pd(111)$ alloy in a "reactive" O_2 atmosphere that Pd segregation is favored by the increase in oxygen chemical potential, which is achieved by increasing the oxygen partial pressure. This finding was experimentally verified in the present work (see Fig. S5). Note that the oxygen chemical potential is inversely related to the temperature, which means that the chemical potential decreases with the increase in the temperature.[47,48] Hence, the PdO_x surface oxide formed on $Ag_{0.98}Pd_{0.02}$ and PdO formed on bulk Pd decompose at a certain temperature because the oxygen chemical potential is not sufficient anymore. The reason why PdO_x on AgPd decomposes at 270 °C lower temperatures compared to PdO on Pd might be the lower stability of PdO_x due to the high solubility of Pd in Ag as well as the lower surface energy of Ag compared to Pd.[68]

For better understanding how the Pd oxide layer on the $Ag_{0.98}Pd_{0.02}$ surface might look, XPS data were quantified, and a model for the Pd oxidation in the alloy was developed; thereby, we assumed that a monolayer thick PdO layer is formed on AgPd.

E. Peak area modeling procedure to estimate the morphology of the PdO_x surface oxide

Let us assume that a homogeneous layer of PdO forms on the alloy surface during oxidation, as visualized in Fig. 9(a).

If this were the case, then the intensity of Pd in the PdO layer can be obtained by integrating from the surface z = 0 to d,[69,70]

$$I^{d}_{\mathrm{PdO}} = I_{0,\mathrm{PdO}}\left[1 - \exp\left(-\frac{d}{\lambda_{\mathrm{PdO,PdO}} \times \cos\alpha}\right)\right], \tag{1}$$

where $I_{0,\mathrm{PdO}}$ is the hypothetical value for an infinitely thick PdO layer and $\lambda_{\mathrm{PdO,PdO}}$ is the effective attenuation length (EAL) of $Pd^{2+}3d_{5/2}$ electrons through PdO. All EAL values in this work were determined by the NIST database[71] using an incident x-ray angle of 56°.

The formula for the intensity of the Pd $3d_{5/2}$ signal from the Pd atoms buried below the oxide film is[69,70]

$$I_{\mathrm{Pd,PdO}} = I_{\infty,\mathrm{Pd}} \exp\left(-\frac{d}{\lambda_{\mathrm{Pd,PdO}}}\right), \tag{2}$$

where $I_{\infty,\mathrm{Pd}}$ is the peak intensity of Pd $3d_{5/2}$ in a homogeneous $Ag_{0.98}Pd_{0.02}$ alloy and $\lambda_{\mathrm{Pd,PdO}}$ is again the effective attenuation length (EAL) of buried $Pd^0 3d_{5/2}$ electrons through PdO.

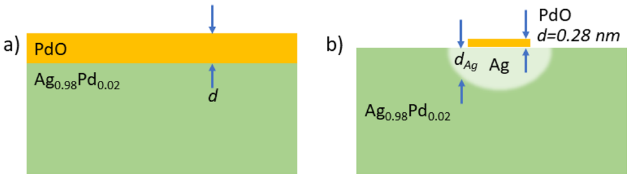

FIG. 9. (a) Schematic of a PdO layer on bulk $Ag_{0.98}Pd_{0.02}$. (b) Schematic of the fractional PdO monolayer coverage of the alloy, including a depletion area below the PdO monolayer, which consists only of Ag atoms.

The different parameters used to apply Eqs. (1) and (2) are discussed in the supplementary material and listed in Table S1.

If we assume a uniform coverage of PdO, as shown in Fig. 10(a), then the calculations from Eq. (1) yield a PdO thickness of 0.022 nm. Given that this number is less than the atomic diameter of Pd, we infer that the assumption of uniform film thickness is not valid. A Pd atom has a diameter of 0.28 nm (covalent diameter). If we assume a layer thickness of 0.28 nm and assume non-uniform coverage, then we arrive at a monolayer coverage of 7.7% (Table S2).

If we now take this updated model, assuming a surface coverage of 7.7%, and use Eq. (2) to calculate the expected metallic Pd 3d peak intensity (assuming a uniform Pd concentration of 2 at. %), we find that the true Pd 3d intensity is substantially lower than the calculated intensity. To explain this discrepancy, we need to add additional sophistication to the model.

The current model does not consider the fact that the Pd incorporated into the PdO film came from diffusion from the underlying alloy. Thus, the underlying alloy should no longer have the full 2% Pd concentration that it started with. If we assume that the volume below the PdO film has been depleted of Pd, we arrive at the model depicted in Fig. 9(b). The Pd-depleted Ag region of such a model is, of course, not trivial to calculate but was approached by implementing a finite element 3D model (see Fig. S7 and Tables S2 and S3 of the supplementary material).

In summary, with the peak intensity modeling procedure, we conclude that the oxidized surface of the AgPd alloy consists of thin, possibly monolayer thick, PdO_x islands with Pd-depleted Ag below and around the islands. Additionally, while we cannot conclusively identify the electronic structure of the oxide, the similarity in binding energy and the qualitative similarity in the peak line shape to PdO suggest that it could be a PdO (Pd^{2+})-like monolayer. An Ag_y–Pd_z–O_x oxide is unlikely, as no correlations between Pd $3d_{5/2}$ oxide and Ag $3d_{5/2}$ oxide were found.

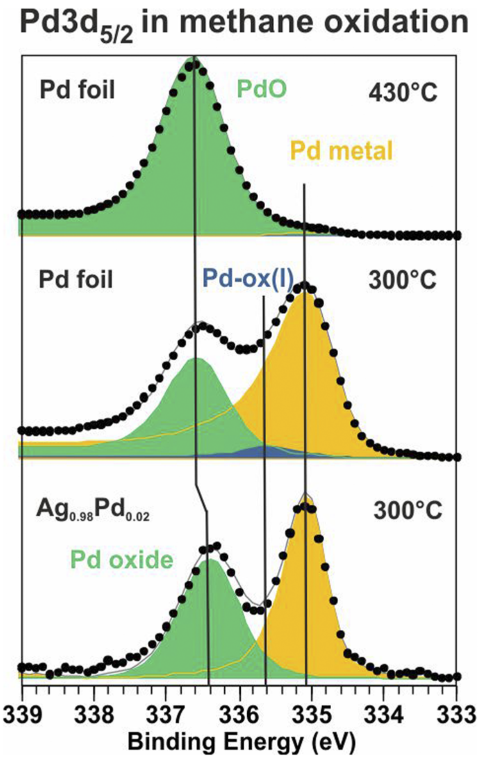

FIG. 10. Electronic structure of the Pd $3d_{5/2}$ states of the Pd foil and the AgPd SAA under methane oxidation conditions.

F. $Ag_{0.98}Pd_{0.02}$ and Pd foil in methane oxidation conditions

After we have intensively discussed the electronic structure of Pd and $Ag_{0.98}Pd_{0.02}$ in oxidative atmospheres, it is of interest to see whether such metastable Pd surface oxides are also present in a reaction mixture that would be used for a catalytic reaction. An oxidative reaction of great economical interest is the total combustion of methane, which is the main component in natural gas and an attractive energy source.[33] Pd was found to be the most active metal of all elements in the complete oxidation of methane. To make the catalytic methane oxidation as energy efficient as possible, low reaction temperatures are desired. So far, Pd requires reaction temperatures above 300 °C to catalyze the total methane oxidation.[32]

It has been shown in the past years of heterogeneous catalysis research that mostly metastable surface species are the active catalytic phases. We therefore examined whether the metastable Pd-oxide phase of $Ag_{0.98}Pd_{0.02}$ is also present under methane oxidation conditions using a reaction mixture of O_2:CH_4:N_2 with a ratio of 5:1:2 (EX6). The measurements reveal that the metastable surface Pd-oxide does indeed form under methane oxidation conditions although the oxygen chemical potential has been reduced by mixing O_2 with CH_4. The surface oxide is the most intense at 300 °C. From this observation, we suggest that AgPd SAA catalysts might be candidates for low temperature methane combustion (≤300 °C).

The electronic structure of $Ag_{0.98}Pd_{0.02}$ in methane oxidation at 300 °C is compared with the polycrystalline Pd under the same conditions (Fig. 10). At 300 °C, the Pd foil is in the transition state between surface oxide and bulk PdO, and when the temperature is further increased (430 °C), bulk PdO has formed (EX7), similar to that observed in a pure O_2 environment.

The results shown here suggest studying the application of SAAs not only for reductive reactions (e.g., hydrogenation reactions) but also for oxidative reactions, since oxidative conditions facilitate the formation of metastable, active surface oxides, as shown for the AgCu SAA system in ethylene epoxidation.[27] During reactive studies, it is important to keep in mind that the reaction atmosphere might change the geometric and electronic environment of the atoms, e.g., adsorbate-induced surface segregation might occur, which could lead to cluster or island formation on SAAs and thus to a loss of the initial single-atom alloy character, as is the case for the AgPd SAA system discussed here. Although in some cases, such catalyst transformation effects may not be desired, in other cases, such metastable surface species could participate in the catalytic performance of single-atom alloys.

IV. CONCLUSION

In this work, an AgPd SAA was studied under oxidative conditions and compared with bulk Pd under similar conditions. We showed by *in situ* XPS spectroscopy that in the case of $Ag_{0.98}Pd_{0.02}$

© Author(s) 2021

SAA, Pd segregates to the surface where it becomes partly oxidized. Through a peak area modeling procedure, we conclude that thin possibly monolayer-thick PdO_x islands form, with Pd-depleted Ag below and around the islands. This two-dimensional surface oxide might be unique for AgPd SAAs since the oxidation of conventional AgPd alloys would lead to phase segregation and nanoparticle formation. The metastable surface oxide on AgPd decomposes at relatively low temperatures (at 320 °C in 1 mbar O_2), which is 270 °C less than the temperature where bulk PdO was observed to decompose. This low decomposition temperature of the PdO_x oxide suggests that the contact with $Ag_{0.98}Pd_{0.02}$ influences the oxide's thermodynamic stability. Since metastable surface species are often the reactive phase of heterogeneous catalysts and because Pd is highly active in the total methane oxidation reaction, we propose that the metastable PdO_x surface oxide on the AgPd SAA could be active in methane oxidation at low temperatures (≤300 °C). We observed that the PdO_x surface oxide is indeed present under methane oxidation conditions.

SUPPLEMENTARY MATERIAL

See the supplementary material for spectroscopic validation of the homogeneous distribution of Pd atoms in the AgPd SAA, further information about the *in situ* oxidation of $Ag_{0.98}Pd_{0.02}$, e.g., the correlation between Oμ5 and S 2p, influence of the O_2 pressure on the Pd surface segregation, and in depth information about the peak area modeling procedure of the PdO_x surface oxide.

ACKNOWLEDGMENTS

We would like to thank the Max Planck Society for the funding and the Helmholtz-Zentrum Berlin for the use of their infrastructure.

DATA AVAILABILITY

The data that support the findings of this study are openly available in Zenodo at https://doi.org/10.5281/zenodo.4482118, https://doi.org/10.5281/zenodo.4482214, and https://doi.org/10.5281/zenodo.4482000.

REFERENCES

[1] R. T. Hannagan, G. Giannakakis, M. Flytzani-Stephanopoulos, and E. C. H. Sykes, Chem. Rev. **120**, 12044 (2020).

[2] F. R. Lucci, M. T. Darby, M. F. G. Mattera, C. J. Ivimey, A. J. Therrien, A. Michaelides, M. Stamatakis, and E. C. H. Sykes, J. Phys. Chem. Lett. **7**, 480 (2016).

[3] Q. Fu and Y. Luo, ACS Catal. **3**, 1245 (2013).

[4] H. L. Tierney, A. E. Baber, J. R. Kitchin, and E. C. H. Sykes, Phys. Rev. Lett. **103**, 1 (2009).

[5] M. B. Boucher, B. Zugic, G. Cladaras, J. Kammert, M. D. Marcinkowski, T. J. Lawton, E. C. H. Sykes, and M. Flytzani-Stephanopoulos, Phys. Chem. Chem. Phys. **15**, 12187 (2013).

[6] G. X. Pei, X. Y. Liu, A. Wang, A. F. Lee, M. A. Isaacs, L. Li, X. Pan, X. Yang, X. Wang, Z. Tai, K. Wilson, and T. Zhang, ACS Catal. **5**, 3717 (2015).

[7] F. R. Lucci, J. Liu, M. D. Marcinkowski, M. Yang, L. F. Allard, M. Flytzani-Stephanopoulos, and E. C. H. Sykes, Nat. Commun. **6**, 1 (2015).

[8] H. Thirumalai and J. R. Kitchin, Top. Catal. **61**, 462 (2018).

[9] G. X. Pei, X. Y. Liu, X. Yang, L. Zhang, A. Wang, L. Li, H. Wang, X. Wang, and T. Zhang, ACS Catal. **7**, 1491 (2017).

[10] C. M. Kruppe, J. D. Krooswyk, and M. Trenary, ACS Catal. **7**, 8042 (2017).

[11] P. Aich, H. Wei, B. Basan, A. J. Kropf, N. M. Schweitzer, C. L. Marshall, J. T. Miller, and R. Meyer, J. Phys. Chem. C **119**, 18140 (2015).

[12] M. Jørgensen and H. Grönbeck, J. Am. Chem. Soc. **141**, 8541 (2019).

[13] M. D. Marcinkowski, M. T. Darby, J. Liu, J. M. Wimble, F. R. Lucci, S. Lee, A. Michaelides, M. Flytzani-Stephanopoulos, M. Stamatakis, and E. C. H. Sykes, Nat. Chem. **10**, 325 (2018).

[14] T. Bligaard and J. K. Nørskov, Electrochim. Acta **52**, 5512 (2007).

[15] B. Hammer and J. K. Nørskov, Adv. Catal. **45**, 71 (2000).

[16] B. Hammer and J. K. Norskov, Nature **376**, 238 (1995).

[17] A. J. Medford, A. Vojvodic, J. S. Hummelshøj, J. Voss, F. Abild-Pedersen, F. Studt, T. Bligaard, A. Nilsson, and J. K. Nørskov, J. Catal. **328**, 36 (2015).

[18] F. Abild-Pedersen, J. Greeley, F. Studt, J. Rossmeisl, T. R. Munter, P. G. Moses, E. Skúlason, T. Bligaard, and J. K. Nørskov, Phys. Rev. Lett. **99**, 4 (2007).

[19] C. J. H. Jacobsen, S. Dahl, B. S. Clausen, S. Bahn, A. Logadottir, and J. K. Nørskov, J. Am. Chem. Soc. **123**, 8404 (2001).

[20] A. Vojvodic and J. K. Nørskov, Natl. Sci. Rev. **2**, 140 (2015).

[21] M. T. Greiner, T. E. Jones, S. Beeg, L. Zwiener, M. Scherzer, F. Girgsdies, S. Piccinin, M. Armbrüster, A. Knop-Gericke, and R. Schlögl, Nat. Chem. **10**, 1008 (2018).

[22] N. Taccardi, M. Grabau, J. Debuschewitz, M. Distaso, M. Brandl, R. Hock, F. Maier, C. Papp, J. Erhard, C. Neiss, W. Peukert, A. Görling, H.-P. Steinrück, and P. Wasserscheid, Nat. Chem. **9**, 862 (2017).

[23] G. Rupprechter, Nat. Chem. **9**, 833 (2017).

[24] M. A. van Spronsen, K. Daunmu, C. R. O'Connor, T. Egle, H. Kersell, J. Oliver-Meseguer, M. B. Salmeron, R. J. Madix, P. Sautet, and C. M. Friend, J. Phys. Chem. C **123**, 8312 (2019).

[25] S. Zafeiratos, S. Piccinin, and D. Teschner, Catal. Sci. Technol. **2**, 1787 (2012).

[26] F. Tao, S. Zhang, L. Nguyen, and X. Zhang, Chem. Soc. Rev. **41**, 7980 (2012).

[27] K. Schweinar, S. Beeg, C. Hartwig, C. R. Rajamathi, O. Kasian, S. Piccinin, M. J. Prieto, L. C. Tanase, D. M. Gottlob, T. Schmidt, D. Raabe, R. Schlögl, B. Gault, T. E. Jones, and M. T. Greiner, ACS Appl. Mater. Interfaces **12**, 23595 (2020).

[28] M. T. Greiner, J. Cao, T. E. Jones, S. Beeg, K. Skorupska, E. A. Carbonio, H. Sezen, M. Amati, L. Gregoratti, M.-G. Willinger, A. Knop-Gericke, and R. Schlögl, ACS Catal. **8**, 2286 (2018).

[29] S. Piccinin, C. Stampfl, and M. Scheffler, Surf. Sci. **603**, 1467 (2009).

[30] R. B. Anderson, K. C. Stein, J. J. Feenan, and L. J. E. Hofer, Ind. Eng. Chem. **53**, 809 (1961).

[31] D. T. Shindell, G. Faluvegi, D. M. Koch, G. A. Schmidt, N. Unger, and S. E. Bauer, Science **326**, 716 (2009).

[32] Z. Li and G. B. Hoflund, J. Nat. Gas Chem. **12**, 153 (2003), https://www.sciengine.com/publisher/scp/journal/JNGC/12/3/10.1016/S1003-9953-2003-12-3-153-160?slug=fulltext.

[33] L. He, J. Bellettre, J. Yue, and L. Luo, Renewable Sustainable Energy Rev. **119**, 109589 (2020).

[34] M. Lyubovsky and L. Pfefferle, Catal. Today **47**, 29 (1999).

[35] E. Lundgren, G. Kresse, C. Klein, M. Borg, J. N. Andersen, M. De Santis, Y. Gauthier, C. Konvicka, M. Schmid, and P. Varga, Phys. Rev. Lett. **88**, 2461031 (2002).

[36] D. Zemlyanov, B. Aszalos-Kiss, E. Kleimenov, D. Teschner, S. Zafeiratos, M. Hävecker, A. Knop-Gericke, R. Schlögl, H. Gabasch, W. Unterberger, K. Hayek, and B. Klötzer, Surf. Sci. **600**, 983 (2006).

[37] H. Gabasch, K. Hayek, B. Klötzer, W. Unterberger, E. Kleimenov, D. Teschner, S. Zafeiratos, M. Hävecker, A. Knop-Gericke, R. Schlögl, B. Aszalos-Kiss, and D. Zemlyanov, J. Phys. Chem. C **111**, 7957 (2007).

[38] R. S. Monteiro, D. Zemlyanov, J. M. Storey, and F. H. Ribeiro, J. Catal. **201**, 37 (2001).

[39] R. Burch, F. J. Urbano, and P. K. Loader, Appl. Catal., A **123**, 173 (1995).

[40] J. N. Carstens, S. C. Su, and A. T. Bell, J. Catal. **176**, 136 (1998).

[41] H. Xiong, M. H. Wiebenga, C. Carrillo, J. R. Gaudet, H. N. Pham, D. Kunwar, S. H. Oh, G. Qi, C. H. Kim, and A. K. Datye, Appl. Catal., B **236**, 436 (2018).

[42] J. J. Willis, A. Gallo, D. Sokaras, H. Aljama, S. H. Nowak, E. D. Goodman, L. Wu, C. J. Tassone, T. F. Jaramillo, F. Abild-Pedersen, and M. Cargnello, ACS Catal. **7**, 7810 (2017).

[43] K. Persson, K. Jansson, and S. G. Järås, J. Catal. **245**, 401 (2007).

© Author(s) 2021

[44] N. M. Kinnunen, J. T. Hirvi, T. Venäläinen, M. Suvanto, and T. A. Pakkanen, Appl. Catal., A **397**, 54 (2011).

[45] A. Hellman, A. Resta, N. M. Martin, J. Gustafson, A. Trinchero, P.-A. Carlsson, O. Balmes, R. Felici, R. Van Rijn, J. W. M. Frenken, J. N. Andersen, E. Lundgren, and H. Grönbeck, J. Phys. Chem. Lett. **3**, 678 (2012).

[46] J. Nilsson, P.-A. Carlsson, S. Fouladvand, N. M. Martin, J. Gustafson, M. A. Newton, E. Lundgren, H. Grönbeck, and M. Skoglundh, ACS Catal. **5**, 2481 (2015).

[47] J. R. Kitchin, K. Reuter, and M. Scheffler, Phys. Rev. B: Condens. Matter Mater. Phys. **77**, 1 (2008).

[48] K. Reuter and M. Scheffler, Phys. Rev. B: Condens. Matter Mater. Phys. **65**, 1 (2002).

[49] A. V. Ruban and H. L. Skriver, Comput. Mater. Sci. **15**, 119 (1999).

[50] A. V. Ruban, H. L. Skriver, and J. K. Nørskov, Phys. Rev. B: Condens. Matter Mater. Phys. **59**, 15990 (1999).

[51] L.-L. Wang and D. D. Johnson, J. Am. Chem. Soc. **131**, 14023 (2009).

[52] M. Salmeron and R. Schlögl, Surf. Sci. Rep. **63**, 169 (2008).

[53] F. Tao and L. Nguyen, Phys. Chem. Chem. Phys. **20**, 9812 (2018).

[54] H. Gabasch, W. Unterberger, K. Hayek, B. Klötzer, E. Kleimenov, D. Teschner, S. Zafeiratos, M. Hävecker, A. Knop-Gericke, R. Schlögl, J. Han, F. H. Ribeiro, B. Aszalos-Kiss, T. Curtin, and D. Zemlyanov, Surf. Sci. **600**, 2980 (2006).

[55] G. Ketteler, D. F. Ogletree, H. Bluhm, H. Liu, E. L. D. Hebenstreit, and M. Salmeron, J. Am. Chem. Soc. **127**, 18269 (2005).

[56] H. Gabasch, E. Kleimenov, D. Teschner, S. Zafeiratos, M. Hävecker, A. Knop-Gericke, R. Schlögl, D. Zemlyanov, B. Aszalos-Kiss, K. Hayek, and B. Klötzer, J. Catal. **242**, 340 (2006).

[57] J. J. Velasco-Vélez, D. Teschner, F. Girgsdies, M. Hävecker, V. Streibel, M. G. Willinger, J. Cao, M. Lamoth, E. Frei, R. Wang, A. Centeno, A. Zurutuza, S. Hofmann, R. Schlögl, and A. Knop-Gericke, Top. Catal. **61**, 2052 (2018).

[58] D. Teschner, J. Borsodi, A. Wootsch, Z. Révay, M. Hävecker, A. Knop-Gericke, S. D. Jackson, and R. Schlögl, Science **320**, 86 (2008).

[59] D. Zemlyanov, B. Klötzer, H. Gabasch, A. Smeltz, F. H. Ribeiro, S. Zafeiratos, D. Teschner, P. Schnörch, E. Vass, M. Hävecker, A. Knop-Gericke, and R. Schlögl, Top. Catal. **56**, 885 (2013).

[60] C. R. O'Connor, M. A. van Spronsen, T. Egle, F. Xu, H. R. Kersell, J. Oliver-Meseguer, M. Karatok, M. Salmeron, R. J. Madix, and C. M. Friend, Nat. Commun. **11**, 1844 (2020).

[61] C. Hartwig, K. Schweinar, T. Jones, S. Beeg, F. Schmidt, R. Schlögl, and M. Greiner, "Isolated Pd atoms in a silver matrix: Spectroscopic and chemical properties," J. Chem. Phys. (submitted) (2021).

[62] E. A. Carbonio, T. C. R. Rocha, A. Y. Klyushin, I. Píš, E. Magnano, S. Nappini, S. Piccinin, A. Knop-Gericke, R. Schlögl, and T. E. Jones, Chem. Sci. **9**, 990 (2018).

[63] T. E. Jones, T. C. R. Rocha, A. Knop-Gericke, C. Stampfl, R. Schlögl, and S. Piccinin, ACS Catal. **5**, 5846 (2015).

[64] T. C. R. Rocha, A. Oestereich, D. V. Demidov, M. Hävecker, S. Zafeiratos, G. Weinberg, V. I. Bukhtiyarov, A. Knop-Gericke, and R. Schlögl, Phys. Chem. Chem. Phys. **14**, 4554 (2012).

[65] T. E. Jones, R. Wyrwich, S. Bo, E. A. Carbonio, M. T. Greiner, A. Y. Klyushin, W. Moritz, A. Locatelli, T. O. Mentes, M. A. Nin, A. Knop-Gericke, R. Schlo, S. Gu, J. Wintterlin, and S. Piccinin, ACS Catal. **8**, 3844 (2018).

[66] C. Heine, B. Eren, B. A. J. Lechner, and M. Salmeron, Surf. Sci. **652**, 51 (2016).

[67] M. Todorova, W. X. Li, M. V. Ganduglia-Pirovano, C. Stampfl, K. Reuter, and M. Scheffler, Phys. Rev. Lett. **89**, 1 (2002).

[68] I. Karakaya and W. T. Thompson, Bull. Alloy Phase Diagrams **9**, 237 (1988).

[69] M. P. Seah, *Practical Surface Analysis* (John Wiley, Chichester, 1983).

[70] C. J. Powell and A. Jablonski, J. Electron Spectros. Relat. Phenomena **178-179**, 331 (2010).

[71] C. J. Powell and A. Jabloski, NIST Effective-Attenuation-Length Database, 1.3 (Gaithersburg, 2011).

© Author(s) 2021